Model validation for radial electric field excitation during L-H transition in JFT-2M tokamak

T. Kobayashi[1], K. Itoh[1,2], T. Ido[1], K. Kamiya[3], S.-I. Itoh[2,4], Y. Miura[5], Y. Nagashima[2,4], A. Fujisawa[2,4], S. Inagaki[2,4], K. Ida[1,2] and K. Hoshino[3]

[1] National Institute for Fusion Science, National Institutes of Natural Sciences, Toki 509-5292, Japan

[2] Research Center for Plasma Turbulence, Kyushu University, Kasuga 816-8580, Japan

[3] National Institutes for Quantum and Radiological Science and Technology, Naka 311-0193, Japan

[4] Research Institute for Applied Mechanics, Kyushu University, Kasuga 816-8580, Japan

[5] Japan Atomic Energy Agency, Naka 311-0193, Japan

E-mail: kobayashi.tatsuya@LHD.nifs.ac.jp

Abstract. In this paper, we elaborate the electric field excitation mechanism during the L-H transition in the JFT-2M tokamak. Using time derivative of the Poisson's equation, models of the radial electric field excitation is examined. The sum of the loss-cone loss current and the neoclassical bulk viscosity current is found to behave as the experimentally evaluated radial current that excites the radial electric field. The turbulent Reynolds stress only plays a minor role. The wave convection current that produces a negative current at the edge can be important to explain the ambipolar condition in the L-mode.

1. Introduction

Comprehensive understanding of the L-H transition mechanism is one of the most important issues towards realization of the future controlled fusion reactors. After the first discovery of the H-mode in the ASDEX tokamak [1], many researchers had attempted to unveil the key physics of the confinement improvement in the H-mode. Thanks to these efforts, the crucial role of the radial electric field was revealed by theoreticians [2, 3] to explain the observed bi-state in the confinement, i.e., the L-mode and the H-mode. Then, the existence of the radial electric field as the edge transport barrier was experimentally confirmed in the JFT-2M [4] and in the DIII-D [5].

The radial electric field in torus plasmas can be excited by several mechanisms even in the quasi-neutral plasmas. For the models of the L-H transition, two of them are mainly treated, i.e., the non-ambipolar particle flux that enhances the radial charge separation and the micro-scale turbulence dynamics [6]. The former is originated by the independent kinetic properties of ions and electrons that are brought by geometrical effects of torus plasmas, including the direct loss-cone loss of the ions across the separatrix [2, 3] and the neoclassical flux of the ions [3, 7]. In contrast, the latter corresponds to the fluctuation induced flow generation, i.e., the turbulent Reynolds stress effects [8] and the wave convection contribution in the momentum transport [2]. These processes can embrace both the electric field excitation and the turbulence suppression during the transition [8]. While, the former only explains the radial electric field excitation and the turbulence damping is undertaken either by the $E \times B$

shearing [9, 10] or by the modulational coupling [11, 12, 13] (see a review [14] for the categorization). In particular, significant progresses in understanding the critical role of the turbulence and the zonal flow on excitation of the radial electric field in the H-mode have been brought in the last decades [11, 15, 16, 17, 18, 19, 20, 21, 22, 23]. Both the neoclassical effect [24] and the bulk viscosity effect [25] were also examined independently. However, to the best of authors' knowledge, few systematic studies that include several possible processes in parallel have ever been reported. Here we examine proposed possible mechanisms for the radial electric field excitation during the L-H transition simultaneously, as an extension of Ref. [26].

In this paper, we elaborate the electric field excitation mechanism during the L-H transition in the JFT-2M tokamak. The radial electric field excitation mechanisms including the direct loss-cone loss, the neoclassical bulk viscosity, and the turbulent Reynolds stress are systematically and quantitatively examined, using a data set obtained with a heavy ion beam probe system. Examining time derivative of the Poisson's equation, the sum of the loss-cone loss current and the neoclassical bulk viscosity current is found to behave as the experimentally observed radial current within a few factors of magnitude. While, the turbulent Reynolds stress only plays a minor role. The wave convection current that produces a negative current at the edge can be important to explain the ambipolar condition in the L-mode. This paper is organized as follows. In section 2, theoretical models of the electric field excitation is overviewed in detail. Section 3 explains the experimental setup in the JFT-2M tokamak. The

main body of the paper showing the experimental results and the discussions for the radial electric field excitation mechanism is given in section 4. Section 5 summarizes the contents of the paper.

2. Theoretical models for electric field excitation

The radial electric field can be excited by the radial current that induces the charge separation. The relation between the radial electric field and the radial current is given by the Poisson equation,

$$\epsilon_\perp \epsilon_0 \frac{\partial E_r}{\partial t} = -J_r, \tag{1}$$

where $\epsilon_\perp$ is the relative dielectric constant of toroidal plasmas [6, 27]. It is given as

$$\epsilon_\perp = 1 + M_{\rm tor}\frac{c^2}{v_{\rm A}^2}, \tag{2}$$

where $c/v_{\rm A}$ denotes the ratio between the speed of light and the Alfvén velocity $v_{\rm A} = B/\sqrt{n_{\rm i} m_{\rm i} \mu_0}$. Inertia enhancement factors $M_{\rm tor}$ in plateau regime and banana regime are given as

$$M_{\rm tor} \sim 1 + 2q^2, \tag{3}$$

and

$$M_{\rm tor} \sim 1 + \frac{1.6q^2}{\sqrt{\epsilon_{\rm t}}}, \tag{4}$$

respectively, where q is the safety factor and $\epsilon_{\rm t} = a/R$ is the inverse aspect ratio. In the toroidal devices, the inertia enhancement factor typically takes the value of several tens. Since $E \times B$ velocity in the poloidal direction has a finite divergence due to the

toroidal geometry, the parallel return flow that maintains the divergence free condition is generated. As a result, the effective acceleration in the poloidal direction is reduced by the factor of $M_{\rm tor}$ [6, 27, 28]. The high speed measurement of the radial electric field with the heavy ion beam probe (HIBP) allows us to evaluate the radial current by Eq. (1). Meanwhile, possible radial currents are modeled theoretically as

$$J_r = J_{\rm i}^{\rm lc} + J_{\rm i}^{\rm bv} - J_{\rm e-i}^{\rm wave} + J_{\rm i}^{v\nabla v} + J_{\rm i}^{\rm CX} + \text{others.} \tag{5}$$

The terms in the r.h.s refer the loss-cone loss current, the neoclassical bulk viscosity current, the wave convection current, the Reynolds stress current, and the charge exchange damping [6]. The charge exchange contribution is assumed to be negligibly small in this discharge, since the edge neutral density is expected to be low enough due to the carbon wall and divertor [29]. Unfortunately, we do not have a data set for the quantitative examination of the charge exchange contribution for this discharge. The first four terms are explicitly given in literatures as a function of the plasma parameters [6]. Nonlinearity of each current term against the radial electric field can provides multiple confinement states and transition between them as shown in Refs. [2, 3]. In the stationary H-mode, the neoclassical contribution is found to be dominant for maintaining the edge radial electric field well in ASDEX-Upgrade [30]. Here, we attempt to clarify the impact of each term during the L-H transition.

The loss-cone loss current $J_{\rm i}^{\rm lc}$ is caused by the direct orbit ion loss across the separatrix. The loss-cone loss current is regulated by the radial electric field since the loss-cone boundary depends on the radial electric field [31]. The loss-cone loss current $J_{\rm i}^{\rm lc}$

is given as a function of the normalized radial electric field, $X \equiv \rho_{\rm p} e E_r / T$ ($\rho_{\rm p} = q\epsilon_{\rm t}^{-1}\rho_{\rm i}$ is the ion gyroradius at the poloidal magnetic field and $\rho_{\rm i}$ is the ion gyroradius) as

$$J_{\rm i}^{\rm lc} = e n_{\rm e} \nu_{\rm ii} \rho_{\rm p} \frac{\nu_*}{\sqrt{\nu_* + X^4 + (r-a)^4 / w_{\rm bi}^4}} \exp\left[-\sqrt{\nu_* + X^4 + (r-a)^4 / w_{\rm bi}^4} \right], \tag{6}$$

where $\nu_* = \nu_{\rm ii} / \omega_{\rm t} \epsilon^{3/2}$ is the ion collisionality defined as a ratio of the ion-ion collision frequency $\nu_{\rm ii}$ and the ion transit angular frequency $\omega_{\rm t}$. The banana width is given as $w_{\rm bi} = q\rho_{\rm i} / \sqrt{\epsilon_{\rm t}} = \sqrt{\epsilon_{\rm t}} \rho_{\rm p}$.

The neoclassical bulk viscosity current $J_{\rm i}^{\rm bv}$ originates in the different trajectories of ions and electrons caused by their mass separation and the magnetic field inhomogeneity along the magnetic field. The neoclassical bulk viscosity current takes a finite value when the condition $X = -\lambda$ violates, where $\lambda \equiv \rho_{\rm p} L_n^{-1}$ is the normalized inverse density gradient length. The expression of $J_{\rm i}^{\rm bv}$ is given as,

$$J_{\rm i}^{\rm bv} = -e n_{\rm e} D_{\rm p} \rho_{\rm p}^{-1} \left(-\lambda - X \right) {\rm Im}\ Z\left(X + i\nu_{\rm ii} / \omega_{\rm t} \right), \tag{7}$$

where $D_{\rm p} = \epsilon_{\rm t} q \rho_{\rm i} T / \sqrt{\pi} r e B$ is a typical diffusivity. Plasma dispersion function ${\rm Im}\ Z\left(X + i\nu_{\rm ii} / \omega_{\rm t} \right)$ is given in Ref. [32] as a similar function of Gaussian $\exp(-X^2)$.

An intuitive model of the wave convection term is given in Ref. [2] as

$$J_{\rm e-i}^{\rm wave} = -e n_{\rm e} D_{\rm e} \rho_{\rm p}^{-1} (-\lambda - X), \tag{8}$$

where $D_{\rm e}$ is the typical turbulent diffusivity and should be a function of E_r. The quasi-linear part of the wave convection term $J_{\rm e-i}^{\rm wave}$ is related to quasi-linear contribution in the Reynolds stress term $J_{\rm i}^{v \nabla v}$ for the case of drift waves [33]. At the L-H transition where the turbulence activity is suppressed by E_r, the value of $D_{\rm e}$ is supposed to sharply

decrease. In the L-mode, the shape of $J_{\mathrm{e-i}}^{\mathrm{wave}}$ resembles to $J_{\mathrm{i}}^{\mathrm{bv}}$ since Im $Z\left(X + iv_{\mathrm{ii}}/\omega_{\mathrm{t}}\right) \sim 1$ when $X \ll 1$.

The the Reynolds stress $\Pi_{r\theta}$ refers the radial transport of the poloidal momentum by turbulent eddies. The turbulent Reynolds stress caused by the radial velocity fluctuation $\tilde{v}_r$ and poloidal velocity fluctuation $\tilde{v}_\theta$ is defined as

$$\Pi_{r\theta} \equiv \langle \tilde{v}_r \tilde{v}_\theta \rangle = -k_r k_\theta S^2 / 2B^2, \tag{9}$$

where S is the turbulent potential fluctuation amplitude. Here S is defined as the potential fluctuation component having a frequency range of 30 kHz $\leq \ f \ \leq$ 90 kHz. The poloidal direction θ is taken in the electron-diamagnetic drift direction following the right-hand rule of the toroidal magnetic field direction (z). Since the velocity fluctuation can be replaced by the potential fluctuation in the magnetized plasma, the transform using the potential fluctuation amplitude S and the turbulence wavenumbers k_r and k_θ works. Note that this transformation includes implicit assumption that the cross coherence between $\tilde{v}_r$ and $\tilde{v}_\theta$ is unity. Therefore, the evaluated $\Pi_{r\theta}$ corresponds to the upper limit of the practical value. The local accumulation of the momentum transport $-r^{-1}\partial r \Pi_{r\theta}/\partial r$ corresponds to the flow acceleration force that can be equivalently rewritten by the form of the radial current $J_{\mathrm{i}}^{v\nabla v}$ as

$$J_{\mathrm{i}}^{v\nabla v} = -e n_{\mathrm{e}} \omega_{\mathrm{ci}}^{-1} r^{-1} \frac{\partial r \Pi_{r\theta}}{\partial r}, \tag{10}$$

where $\omega_{\mathrm{ci}} = eB/m_{\mathrm{i}}$ is the ion gyro angular frequency.

3. Experimental setup

The models of the radial current shown above are examined one by one using the experimental data obtained in the JFT-2M tokamak. Dimension of the JFT-2M plasma is a major radius (R) of 1.3 m and an averaged minor radius (a) of 0.3 m. The neutral beam (NB) of the power of $P_{\rm NB} = 750$ kW is injected into the low density plasma at the line averaged electron density of $\bar{n}_{\rm e} = 1.1 \times 10^{19}$ m^{-3}. The toroidal confinement magnetic field is set to $B = 1.17$ or 1.28 T. An upper single-null divertor configuration is employed, where the ∇B drift of ions is directed toward the X-point and the safety factor at the flux surface enclosing 95% of the total poloidal flux, q_{95}, is 2.9. The plasma current $I_{\rm p}$ is 190 kA. The present experimental condition corresponds to the marginal condition for the L-H transition, i.e., slightly above the threshold heating power. At the plasma edge, the ion collisionality is slightly below unity so that the neoclassical transport is in the banana regime. The inertia enhancement factor at the edge is $M_{\rm tor} \sim 30$. JFT-2M has been shutdown in 2004.

The heavy ion beam probe (HIBP) provides the electrostatic potential ϕ and the electron density $n_{\rm e}$ at four sample volumes (6 mm $\times$ 2 mm) simultaneously, with a sampling time of 1 μs [34, 35]. The distances between channels projected on the outer mid-plane are ~ 2.5 mm. The two key parameters of the model validation, i.e., the radial electric field $E_r \equiv -\partial\phi/\partial r$ and the inverse density gradient length $L_n^{-1} \equiv -n_{\rm e}^{-1}\partial n_{\rm e}/\partial r$, are evaluated by taking the difference of two HIBP signals measured at neighboring sample volumes. In the series of experiments, the radial positions of the HIBP sample

volumes were scanned in the edge region (-5 cm $< r - a < 0$ cm, where $r - a$ is the radial distance from the saparatrix), in a shot-to-shot basis. The bandwidth of the measurement is up to 100 kHz so that simultaneous measurement of the mean profile and the turbulent fluctuation is feasible.

4. Experimental results

4.1. Basic observations

Figures 1 (a)-(c) overview the time evolution of the D_α intensity, the potential at the location of the radial electric field well in the H-mode, $r - a \sim -1$ cm (see the radial profile of E_r in Fig. 3), and the wavelet power spectrum density of ϕ for the target discharge #90055. The NB is injected from $t = 0.7$ s and the L-H transition occurs at $t_{\rm LH} \sim 0.734$ s (dashed vertical line in Fig. 1), where the rapid drops of D_α and ϕ are seen [26]. In the early stage of the L-mode in 0.7 s $< t <$ 0.715 s, the geodesic acoustic mode (GAM) is observed at $f \sim 15$ kHz as a coherent spectral peak [34, 35]. A few tens millisecond before the transition, the GAM activity disappears and a low frequency fluctuation power increases in $f < 5$ kHz. This low frequency perturbation in the potential is regarded as the limit cycle oscillation (LCO), which refers the quasi-periodic repetition of the L-H transition [36, 37]. The LCO in JFT-2M is characterized by a relatively smaller amplitude of the D_α perturbation. Radial profiles of the parameters such as the density and the potential during the LCO phase are similar to those in the L-mode phase, where the density pedestal formation is not completed. There is

an interplay among the turbulence, the radial electric field, and the density gradient, exhibiting the periodical formation and the deformation of the small edge transport barrier at the LCO frequency [36]. See a variety of the LCO characteristics in Ref. [38]. The onset of the LCO is somewhat ambiguous in this discharge. After the L-H transition, there can be seen another low frequency ELM type oscillation at $f < 1$ kHz [39].

Focusing on the dynamics of the L-H transition, the detailed time trace of D_α, the soft-x-ray (SX) emissions and the HIBP measured quantities (E_r, L_n^{-1} and J_r) for the instance of the transition is given in Fig. 2 at the location where the transport barrier is strongest. In order to clearly observe the time evolution of the mean parameters reducing the noise component, all spatial channels of the HIBP are averaged, after which a numerical low-pass filter having a cutoff frequency of 2 kHz is operated. As discussed in Ref. [36], the LCO does not directly account for the trigger of the L-H transition. The mean plasma parameters and the turbulence characteristics in the LCO phase are similar to these in the L-mode phase [37]. The L-H transition seems to be triggered by the reach of the sawtooth heat pulse at the edge, as shown in the SX emissions. The radial electric field at the edge transport barrier drops within less than 100 μs. After the first drop of the radial electric field, there exists $\sim$ 2 ms of a meta-stable state in 1 ms $\leq t \leq$ 3 ms, which we call the 'MH-mode'. Then, the second drop in the radial electric field appears with a longer period of $\sim$ 1 ms and the plasma reaches the final 'H-mode'. The increase of the density gradient also emerges at both steps. The bottom trace of Fig. 2 (c) is the evaluated radial current using Eq. (1). During the first L-MH

transition, the positive current takes the largest peak of ~ 3.5 A/m^2. In addition, the second smaller peak is also seen at the MH-H transition.

There are 5 discharges having a high reproducibility and different HIBP measurement range, from which the radial profiles in each confinement state can be determined. Shown in Fig. 3 is the radial profile of the radial electric field. Green symbols show the mean values of each measurement point in the H-mode where the different symbols come from different discharges. Width of the curves represent the scatter of the values from the fifth-degree polynomial fitting curve. The L-mode profile shown in the blue curves is characterized by a low radial electric field. At the L-MH transition, the radial electric field well of -10 kV/m emerges, and deepens to -25 kV/m at the final MH-H transition.

4.2. Model validation for radial electric field excitation mechanism

Validation of the theoretical models is discussed by comparing the modeled J_r and the experimentally evaluated J_r, following the framework performed in Ref. [24]. First, let us examine the loss-cone loss current $J_{\rm i}^{\rm lc}$ and the neoclassical bulk viscosity current $J_{\rm i}^{\rm bv}$ given by Eqs. (6) and (7), respectively. Figure 4 shows the possible values the radial current expected by the loss-cone loss process and by the neoclassical bulk viscosity process as functions of the normalized radial electric field X and the normalized inverse density gradient length λ. Although $J_{\rm i}^{\rm lc}$, $J_{\rm i}^{\rm bv}$ and X are functions of the ion temperature $T_{\rm i}$ too, we first do not take into account the change of $T_{\rm i}$ during the transition for

simplicity. Possible uncertainty due to the change of T_i is discussed below. Note that by surveying the ambipolar condition using these two terms, a model that predicts the existence of the bi-state of the radial electric field, i.e., the L-mode and the H-mode, was developed [3]. The black curve shows the trajectory of the experimental parameters shown in Fig. 2 (c). The expected radial currents based on these models are the values of Fig. 4 on the trajectory. Figure 5 shows the time evolutions of J_i^lc and J_i^bv as well as the experimentally evaluated radial current based on Eq. (1). The loss-cone loss current is shown to take a positive value of ~ 2 A/m^2 in the L-mode, which sharply disappears after the L-MH transition. The neoclassical bulk viscosity current is composed of two terms, i.e., the gradient contribution $J_\mathrm{i}^{\mathrm{bv},L_\mathrm{n}^{-1}}$ and the radial electric field contribution $J_\mathrm{i}^{\mathrm{bv},E_r}$. Positive value of λ corresponds to the positive radial current, that enhances the negative growth of the radial electric field. The excited radial electric field contributes the negative radial current in turn. The net neoclassical bulk viscosity current takes a positive value of ~ 4 A/m^2 in the L-mode. During the transition, the neoclassical bulk viscosity current shows a rather gradual decay. The sum of these two terms is shown in Fig. 5 (c) with the experimentally evaluated radial current. The two curves show a good agreement in 0.5 ms $< t - t_\mathrm{LH} <$ 1 ms in terms of the absolute value of the current and the time scale of the change, during the L-MH transition. Note that a peak in the $J_\mathrm{i}^\mathrm{lc} + J_\mathrm{i}^\mathrm{bv}$ curve at $t - t_\mathrm{LH} \sim -0.3$ ms is not a meaningful event for the transition but just a perturbation of the parameter. The transition happens without these peaks in a different discharge. In the model current, a large positive offset is seen in the L-mode,

and no current peak at the MH-H transition ($t - t_{\mathrm{LH}} \sim 3.5$ ms) appears.

Figure 6 shows the radial current as a function of the normalized radial electric field X. The black curve indicates the experimental value of J_r evaluated using Eq. (1). Each (quasi-) stationary state, i.e., the L-mode, the MH-mode, and the H-mode, corresponds to the trajectory at $J_r = 0$, as indicated by the labels. At the L-MH transition, the positive radial current is excited that induces the negative growth of the radial electric field. At a point $X \sim 0.7$, the radial current turns to decrease down to zero, and the plasma goes to the MH-mode. Two millisecond after, again the positive radial current is excited, which further deepens the radial electric field. The trajectory of the radial current against the normalized radial electric field is compared to the sum of $J_{\mathrm{i}}^{\mathrm{lc}}$ and $J_{\mathrm{i}}^{\mathrm{bv}}$ shown by the red curve. The shaded area in Fig. 6 (a) is the uncertainty of $J_{\mathrm{i}}^{\mathrm{lc}} + J_{\mathrm{i}}^{\mathrm{bv}}$, which comes from the uncertainty of the ion temperature determination during the transition. The time resolution of the ion temperature signal measured with the charge exchange recombination spectroscopy system is far slower than the time scale of the L-H transition. Here, we evaluate the uncertainty of the values of $J_{\mathrm{i}}^{\mathrm{lc}}$ and $J_{\mathrm{i}}^{\mathrm{bv}}$ by taking into account the possible range of time evolution of the ion temperature. Two extreme limits are that, $\partial T_{\mathrm{i}}/\partial t = 0$ and $T_{\mathrm{i}} \propto T_{\mathrm{e}}$, where the electron cyclotron emission system is used for estimating an edge electron temperature T_{e}. The lower and upper boundaries of the red shaded area correspond to the cases $\partial T_{\mathrm{i}}/\partial t = 0$ and $T_{\mathrm{i}} \propto T_{\mathrm{e}}$, respectively. The normalized radial electric field is evaluated under the assumption of $\partial T_{\mathrm{i}}/\partial t = 0$ for simplicity. At the L-MH transition at $X \sim -1$, $J_{\mathrm{i}}^{\mathrm{lc}} + J_{\mathrm{i}}^{\mathrm{bv}}$ is in agreement with the

observation within the factor of ~ 2. The peak in the $E_r - J_r$ curve at $X \sim -2$ for the MH-H transition is not clearly predicted by $J_{\rm i}^{\rm lc} + J_{\rm i}^{\rm bv}$, since the established models are not focused on such a multi-step transition. Moreover, in the L-mode, a finite positive offset of the radial current $\sim +6$ A/m^2 is predicted by $J_{\rm i}^{\rm lc} + J_{\rm i}^{\rm bv}$ even in the stationary state, $\partial E_r/\partial t = 0$, while the experimentally obtained value shows $J_r = 0$. Figures 6 (b) and (c) plot each term of $J_{\rm i}^{\rm lc}$ and $J_{\rm i}^{\rm bv}$ in addition to the experimentally obtained J_r and the prediction of $J_{\rm i}^{\rm lc} + J_{\rm i}^{\rm bv}$ under the cases of $\partial T_{\rm i}/\partial t = 0$ and $T_{\rm i} \propto T_{\rm e}$, respectively. Contributions from $J_{\rm i}^{\rm bv}$ and $J_{\rm i}^{\rm lc}$ seem to be in the same order in the case $\partial T_{\rm i}/\partial t = 0$, meanwhile under the case $T_{\rm e} \propto T_{\rm i}$ the contribution of $J_{\rm i}^{\rm bv}$ dominates over that of $J_{\rm i}^{\rm lc}$.

Figure 7 shows the time evolution of the difference between the experimentally evaluated radial current and the sum of the loss-cone loss current and the neoclassical bulk viscosity current. It is shown that the other current source is necessary to satisfy the ambipolar condition in the L-mode. A possible candidate to compensate the excess prediction of the radial current by $J_{\rm i}^{\rm lc} + J_{\rm i}^{\rm bv}$ is the wave convection current $J_{\rm e-i}^{\rm wave}$. Here we qualitatively evaluate this current according to the given intuitive formula Eq. (8). For the present plasma parameters, the polarity of $J_{\rm e-i}^{\rm wave}$ is negative, and its absolute value is in the same order with $J_{\rm i}^{\rm bv}$ under the assumption that $D_{\rm p}$ in Eq. (7) and $D_{\rm e}$ in Eq. (8) take values in the same order. This can make the modeled radial current to be zero in the L-mode. At the onset of the transition, turbulence is rapidly suppressed by E_r, and the value of $D_{\rm e}$ is supposed to sharply decrease. Therefore, the previous discussion is not altered by this term in the MH-mode and the H-mode. Exploration of

more precise model of the wave convection contribution that is subject to the qualitative validation has been undertaken, in order to conclude the discussion.

Next, the contribution of the Reynolds stress current is discussed. Figure 8 shows the radial profiles of the turbulent Reynolds stress and the obtained Reynolds stress force and the corresponding Reynolds stress current $J_{\rm i}^{v\nabla v}$ in the L-mode. At the radius of the transport barrier $r-a \sim -0.6$ cm, the expected radial current is only -0.2 A/m^2, which is one order smaller than either $J_{\rm i}^{\rm lc}$ or $J_{\rm i}^{\rm bv}$. Therefore, the Reynolds stress current only plays a minor role in the L-mode. The turbulence intensity is reduced due to the large electric field in the MH-mode and H-mode so that the lesser impact of the Reynolds stress is expected after the L-MH transition. At the plasma boundary, a large value of $J_{\rm i}^{v\nabla v}$ is observed. The Reynolds stress sharply changes at the very edge region since the radial wavenumber is modified by the plasma boundary. The examination of the ambipolar condition at the plasma boundary is relevant subject for the plasma edge modeling.

The minor role of the Reynolds stress is also confirmed during the LCO period [36, 37]. Figures 9 (a)-(c) show the conditional averaged time evolution of the radial electric field, the turbulence amplitude, and the Reynolds stress for one LCO period. Note that the sign of the mean Reynolds stress is different from that in Refs. [36, 37] since the definition of the poloidal direction is different. The Reynolds stress modulation is evaluated as

$$\hat{\Pi}_{r\theta} \sim \Pi_{r\theta}[1 + 2\hat{S}/S + \hat{k}_r/k_r + \hat{k}_\theta/k_\theta], \tag{11}$$

where hats indicate the fluctuation quantities at the LCO frequency and $\Pi_{r\theta}$ is mean Reynolds stress given by Eq. (9). The Reynolds stress driven radial electric field modulation is estimated by Eqs. (1) and (10). Amplitude of the Reynolds stress modulation monotonically decreases toward the edge and disappears at the separatrix [37], thus the substitution of the spatial derivative by the difference, $|r^{-1}\partial r\Pi_{r\theta}/\partial r| = |\Pi_{r\theta}|(a-r)^{-1}$, is operational. The expected radial electric field modulation amplitude is then given as

$$\delta|\hat{E}_r| = -\frac{1}{\omega_{\rm LCO}}\frac{1}{\epsilon_\perp\epsilon_0}\hat{J}_{\rm i}^{v\nabla v} \sim -\frac{B}{M_{\rm tor}\omega_{\rm LCO}}\frac{|\hat{\Pi}_{r\theta}|}{a-r}, \tag{12}$$

where $\omega_{\rm LCO}$ is the angular frequency of the LCO. The r.h.s of the equation is calculated with the parameters of $\omega_{\rm LCO} \sim 3\times10^4$ s^{-1}, $M_{\rm tor} \sim 30$ for $q \sim 3$ and $|\hat{\Pi}_{r\theta}|(a-r)^{-1} \sim 10^7$ m/s^2 as $\delta|\hat{E}_r| \sim 10$ kV/m. The Reynolds stress driven $\hat{E}_r$ is one order smaller than the observed $\hat{E}_r \sim 500$ m/s, which indicates the minor role of the Reynolds stress. The Lissajous diagram between $|E_r|$ and S is shown in Fig. 9 (d) in order to investigate the causal relation between them. The direction of the rotation is the counter clockwise, i.e., the increase of $|E_r|$ precedes the increase of S. Therefore, the majority of the radial electric field modulation should be caused by the other player than the turbulent Reynolds stress. These discussions are consistent with the observation during the L-MH transition.

5. Summary

In this paper, we elaborated the radial electric field excitation mechanism based on the JFT-2M experimental data. The radial electric field excitation mechanisms including the direct loss-cone loss, the neoclassical bulk viscosity, and the turbulent Reynolds stress were systematically and quantitatively examined, using a data set obtained with a heavy ion beam probe system. Examining time derivative of the Poisson's equation, the sum of the loss-cone loss current and the neoclassical bulk viscosity current was found to behave as the experimentally observed radial current within a few factors of magnitude. The turbulent Reynolds stress was shown to play a minor role. The wave convection current that produces a negative current at the edge can be important to explain the ambipolar condition in the L-mode.

Acknowledgments

We thank Drs. P. H. Diamond, G. R. Tynan, U. Stroth, J.-Q. Dong, K. J. Zhao, C. Hidalgo, M. Sasaki, and Y. Kosuga for useful discussions, and the late H. Maeda, Y. Hamada, M. Mori, Y. Kamada, and S. Sakakibara for strong support. This work is partly supported by the Grant-in-Aid for Scientific Research of JSPS, Japan (23244113, 15H02155, 26887047, 16H02442), collaboration programs with JAEA and the RIAM of Kyushu University, and the Asada Science Foundation.

Reference

[1] F Wagner *et al* 1982 *Phys. Rev. Lett.* **49** 1408–1412

[2] S-I Itoh and K Itoh 1988 *Phys. Rev. Lett.* **60** 2276–2279

[3] K C Shaing and E C Crume Jr 1989 *Phys. Rev. Lett.* **63** 2369

[4] K Ida *et al* 1990 *Phys. Rev. Lett.* **65** 1364–1367

[5] R J Groebner, K H Burrell, and R P Seraydarian 1990 *Phys. Rev. Lett.* **64** 3015

[6] K Itoh and S-I Itoh 1996 *Plasma Phys. Control. Fusion* **38** 1

[7] T E Stringer *et al* 1993 *Nucl. Fusion* **33** 1249

[8] E J Kim and P H Diamond 2003 *Phys. Rev. Lett.* **90** 185006

[9] H Biglari, P H Diamond, and P W Terry 1990 *Phys. Fluids B* **2** 1

[10] S-I Itoh and K Itoh 1990 *J. Phys. Soc. Jpn.* **59** 3815

[11] P H Diamond, S-I Itoh, K Itoh, and T S Hahm 2005 *Plasma Phys. Control. Fusion* **47** R35

[12] K Itoh, S-I Itoh, K Kamiya, and N Kasuya 2015 *Plasma Phys. Control. Fusion* **57** 075008

[13] K Itoh, S-I Itoh, K Kamiya, and T Kobayashi 2017 *Nucl. Fusion* **57** 022005

[14] P W Terry 2000 *Revi. Mod. Phys.* **72** 109

[15] A Fujisawa, K Itoh, H Iguchi, K Matsuoka, S Okamura, A Shimizu, T Minami, Y Yoshimura, K Nagaoka, C Takahashi, *et al* 2004 *Phys. Rev. Lett.* **93** 165002

[16] T Estrada *et al* 2010 *Europhys. Lett.* **92** 35001

[17] L Schmitz *et al* 2012 *Phys. Rev. Lett.* **108** 155002

[18] P Manz, G S Xu, B N Wan, H Q Wang, H Y Guo, I Cziegler, N Fedorczak, C Holland, S H Müller, S C Thakur, *et al* 2012 *Phys. Plasmas* **19** 072311

[19] I Shesterikov, Y Xu, *et al* 2013 *Phys. Rev. Lett.* **111** 055006

[20] Z Yan, G R McKee, R Fonck, P Gohil, R J Groebner, and T H Osborne 2014 *Phys. Rev. Lett.* **112** 125002

[21] G Y Park, S S Kim, Hogun Jhang, P H Diamond, T Rhee, and X Q Xu 2015 *Phys. Plasmas* **22**

032505

[22] L Chôné, P Beyer, Y Sarazin, G Fuhr, C Bourdelle, and S Benkadda 2014 *Phys. Plasmas* **21** 070702

[23] G R Tynan, I Cziegler, P H Diamond, M Malkov, A Hubbard, J W Hughes, J L Terry, and J H Irby 2016 *Plasma Phys. Control. Fusion* **58** 044003

[24] A Fujisawa *et al* 1997 *Phys. Rev. Lett* **79** 1054

[25] S Kitajima, H Takahashi, Y Tanaka, H Utoh, M Sasao, M Takayama, K Nishimura, S Inagaki, and M Yokoyama 2006 *Nucl. Fusion* **46** 200

[26] T Kobayashi, K Itoh, T Ido, K Kamiya, S-I Itoh, Y Miura, Y Nagashima, A Fujisawa, S Inagaki, K Ida, *et al* 2016 *Sci. Rep.* **6** 30720

[27] M N Rosenbluth and F L Hinton 1998 *Phys. Rev. Lett.* **80** 724–727

[28] M Honda and A Fukuyama 2016 *Comput. Phys. Commun.* **208** 117–134

[29] K Itoh and S-I Itoh 1995 *Plasma Phys. Control. Fusion* **37** 491

[30] E Viezzer, T Pütterich, C Angioni, A Bergmann, R Dux, E Fable, RM McDermott, U Stroth, E Wolfrum, *et al* 2013 *Nucl. Fusion* **54** 012003

[31] S-I Itoh and K Itoh 1989 *Nucl. Fusion* **29** 1031

[32] B D Fried and S D Conte. *The Plasma Dispersion Function.* New York: Academic, 1961.

[33] P H Diamond and Y-B Kim 1991 *Phys. Fluids B* **3** 1626

[34] T Ido *et al* 2006 *Plasma Phys. Control. Fusion* **48** S41

[35] T Ido *et al* 2006 *Nucl. Fusion* **46** 512

[36] T Kobayashi, K Itoh, T Ido, K Kamiya, S-I Itoh, Y Miura, Y Nagashima, A Fujisawa, S Inagaki, K Ida, *et al* 2013 *Phys. Rev. Lett.* **111** 035002

[37] T Kobayashi, K Itoh, T Ido, K Kamiya, S-I Itoh, Y Miura, Y Nagashima, A Fujisawa, S Inagaki, K Ida, *et al* 2014 *Nucl. Fusion* **54** 073017

[38] K Itoh, S-I Itoh, and A Fujisawa 2013 *Plasma Fusion Res.* **8** 1102168

[39] T Kobayashi, K Itoh, T Ido, K Kamiya, S-I Itoh, Y Miura, Y Nagashima, A Fujisawa, S Inagaki,

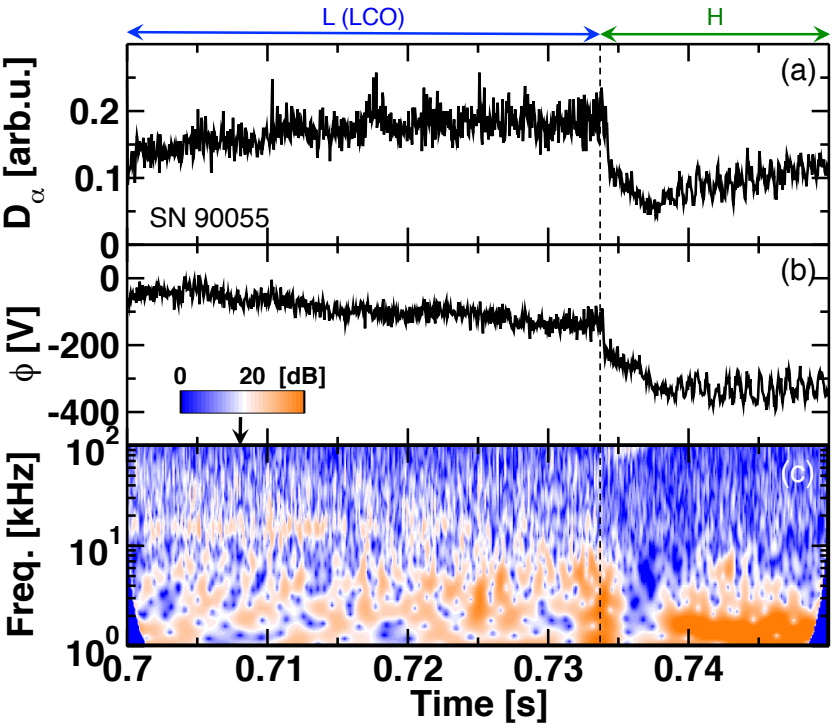

Figure 1. Time evolutions of (a) the D_α intensity, (b) the potential at $r - a \sim -1$ cm and (c) the wavelet power spectrum density of the potential fluctuation.

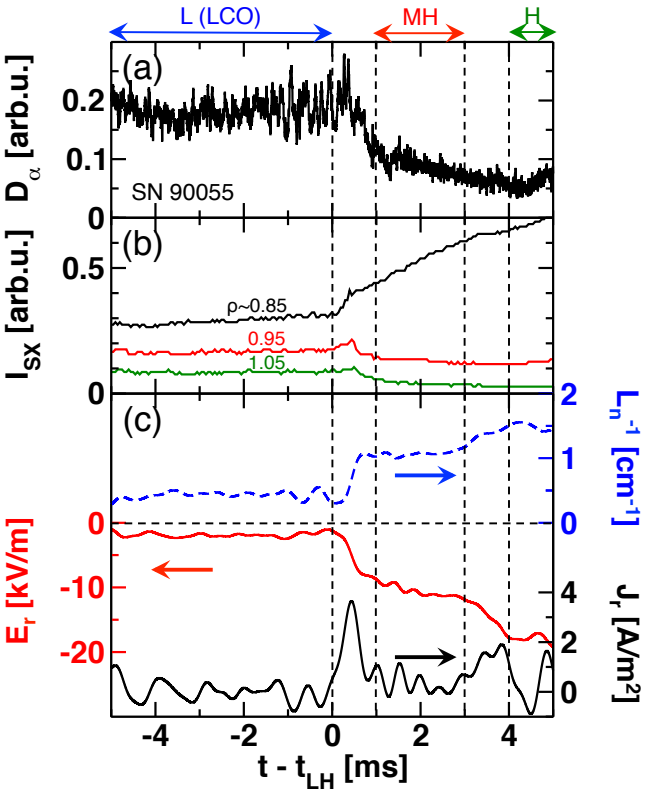

Figure 2. Time evolutions of (a) the D_α intensity, (b) the soft-x-ray emission and (c) the inverse density gradient length, the radial electric field, and the radial current.

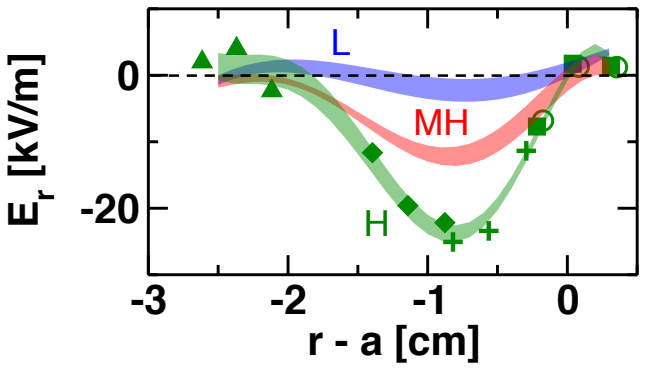

Figure 3. Radial profile of the radial electric field for the L-mode (blue), the MH-mode (red) and the H-mode (green).

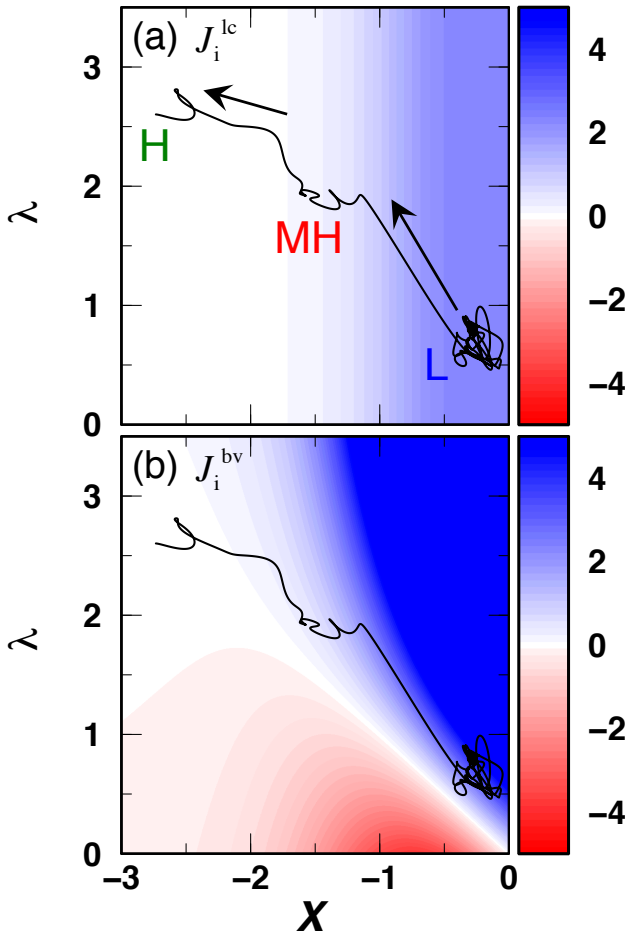

Figure 4. Theoretical prediction of the radial currents excited by (a) the loss-cone loss process and by (b) the neoclassical bulk viscosity process as functions of the normalized radial electric field X and the normalized inverse density gradient length λ.

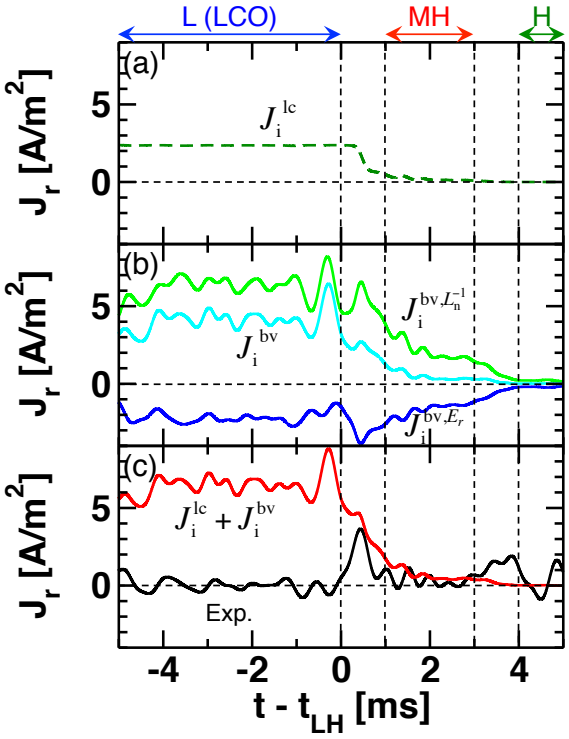

Figure 5. Time evolutions of (a) the loss-cone loss current, (b) the neoclassical bulk viscosity current, and (c) the sum of (a) and (b) as well as the experimentally evaluated radial current.

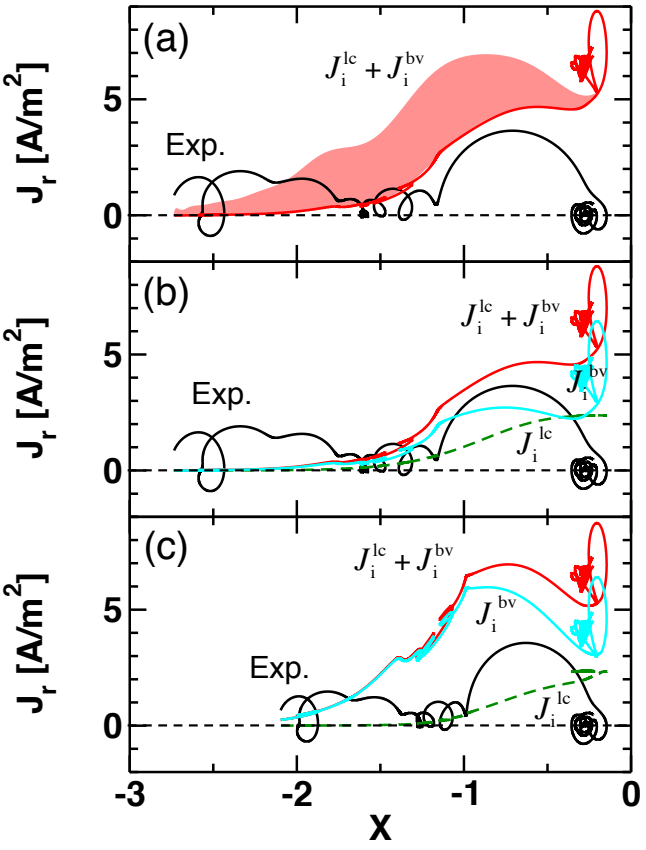

Figure 6. (a) The evaluated radial current and the radial current predicted by the sum of the loss-cone loss current and the neoclassical bulk viscosity current as a function of the normalized radial electric field. The evaluated radial current and the radial current predicted by the models in the different assumption of the ion temperature, (b) $\partial T_i/\partial t = 0$ and (c) $T_i \propto T_e$.

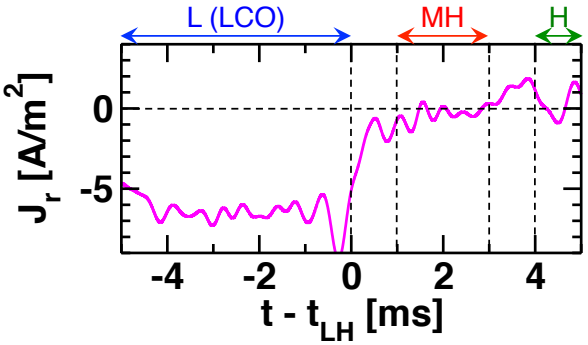

Figure 7. Time evolution of the difference between the experimentally evaluated radial current and the sum of the loss-cone loss current and the neoclassical bulk viscosity current.

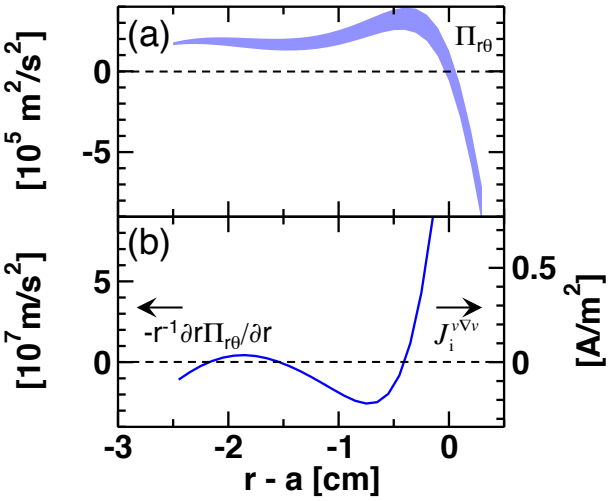

Figure 8. Radial profiles of (a) the Reynolds stress and (b) the Reynolds force and corresponding radial current for the case of L-mode.

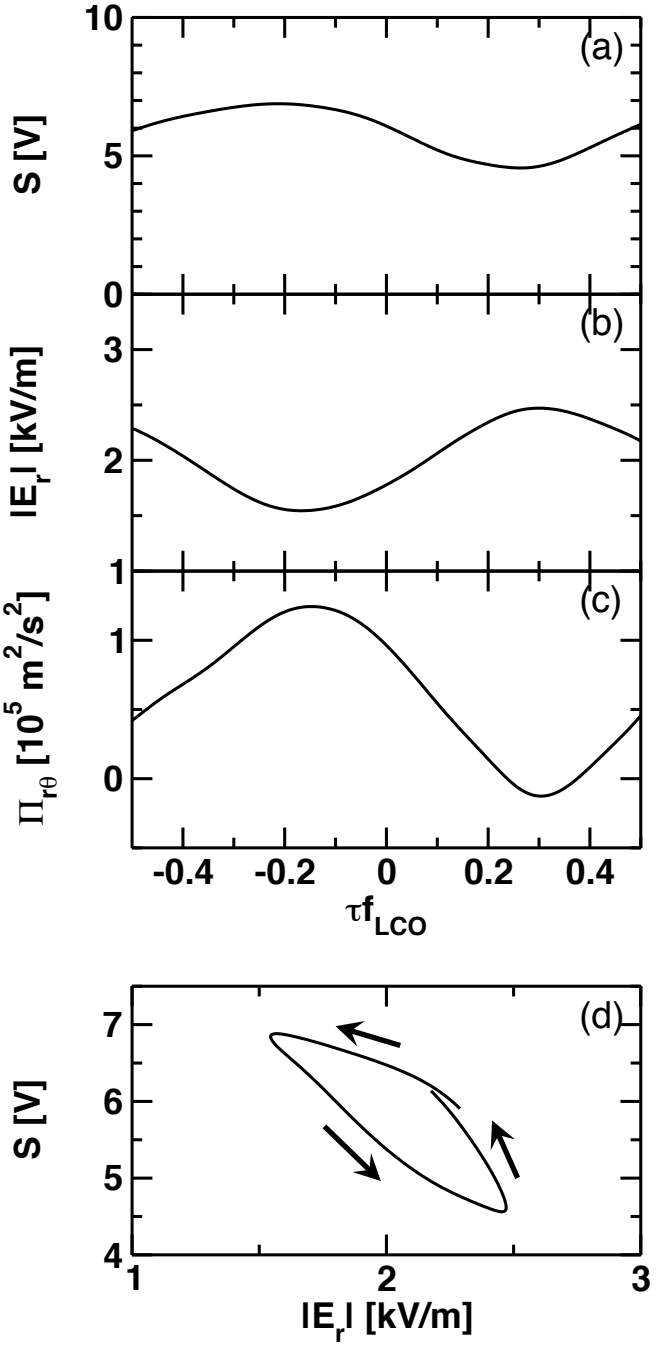

Figure 9. Conditional averaged time evolutions of (a) the turbulence amplitude in the potential fluctuation (b) the absolute value of the radial electric field and (c) the Reynolds stress, plotted as a function of the LCO phase. (d) Lissajous diagram between the turbulence amplitude and the absolute value of the radial electric field.